Fabrication of a Silica Coating on Magnetic γ-Fe_2O_3 Nanoparticles by an Immobilized Enzyme

Mohammed Ibrahim Shukoor,[†] Filipe Natalio,[‡] Helen Annal Therese,[†] Muhammad Nawaz Tahir,[†] Vadim Ksenofontov,[†] Martin Panthöfer,[†] Marc Eberhardt,[§] Patrick Theato,[§] Heinz Christoph Schröder,[‡] Werner E. G. Müller,[‡] and Wolfgang Tremel*[,†]

Institut für Anorganische Chemie and Analytische Chemie, Universität Mainz, Duesbergweg 10-14, D-55099 Mainz, Germany, Institut für Physiologische Chemie, Abteilung Angewandte Molekularbiologie, Universität Mainz, Duesbergweg 6, D-55099 Mainz, Germany, and Institut für Organische Chemie, Universität Mainz, Duesbergweg 10-14, D-55099 Mainz, Germany

Received October 17, 2007. Revised Manuscript Received March 16, 2008

Silicatein, a hydrolytic protein encountered in marine sponges, was immobilized on maghemite (γ-Fe_2O_3) nanoparticles that were surface functionalized with a reactive mulfunctional polymer. This polymer carries an anchor group based on dopamine which is capable of binding to the γ-Fe_2O_3 surface and a reactive functional group which allows binding of various biomolecules onto inorganic nanoparticles. This functional nitrilotriacetic acid (NTA) group allows immobilization of His-tagged silicatein on the surface of the γ-Fe_2O_3 nanoparticles. The surface-bound protein retains its native hydrolytic activity to catalyze formation of silica through copolymerization of alkoxysilanes $Si(OR)_4$. Functionalization of the magnetic nanoparticles and the architecture of the SiO_2-coated γ-Fe_2O_3 nanoparticles was confirmed by TEM studies as well as by FT-IR and optical microscopy.

Introduction

The importance of nanocomposites built on different inorganic or organic components is increasingly recognized because they can acquire intriguing multifunctional properties that can be tailored and tuned. As an example, nonmagnetic semiconductor nanocrystals with an optical band gap determined by dot size, such as CdSe quantum dots, can be mixed with magnetic nanocrystals, such as γ-Fe_2O_3 (maghemite) dots, to form a novel magnetooptic material.[1] Although mixtures of different types of nanocrystals may be formed, for example, by spin casting, such hybrid materials usually have poor properties. A more successful approach has been to deposit a concentric mantle on the outside of spherical nanoparticles to fabricate core−shell nanostructures. A typical example for solids is encapsulation of CdSe nanoparticles in a shell of ZnS to tailor the photophysical properties.[2] Magnetic nanoparticles[3] are emerging as a new technology in biomedical applications for clinical diagnostics and in vivo applications such as magnetic resonance imaging (MRI) of tumors, hyperthermia treatment for cancer cells,[4] magnetically assisted drug delivery,[5] or clinical diagnostics.[6] Coatings protect nanoparticles from reaction with the external environment and simultaneously serve as a medium for the subsequent particle functionalization to render them chemically functional and simultaneously physiologically compatible for biomedical applications. As an example, iron oxide particles have been encapsulated with noble metals (e.g., Au)[7] or silica.[8] A key challenge for future bioapplications of nanomaterials is the development of a versatile surface chemistry that provides stability and solubility under physiological conditions, endows detectability, and at the same time allows targeting, e.g., for magnetic resonance imaging (MRI) or magnetically assisted drug delivery. A general route that simultaneously addresses all these requirements would be a significant advancement.

* To whom correspondence should be addressed. Phone: +49-6131-392-5135. Fax: +49-6131-392-5605. E-mail: tremel@uni-mainz.de.
[†] Institut für Anorganische Chemie and Analytische Chemie.
[‡] Institut für Physiologische Chemie, Abteilung Angewandte Molekularbiologie.
[§] Institut für Organische Chemie.

(1) (a) Redl, F. X.; Cho, K.-S.; Murray, C. B.; Brien, S. O. *Nature* **2003**, *423*, 968–971. (b) Brust, M.; Kiely, C. J. *Colloid Surf. A* **2002**, *202*, 175–186.
(2) (a) Dabbousi, B. Q.; Rodriguez-Viejo, J.; Mikulec, F. V.; Heine, J. R.; Mattoussi, H.; Ober, R.; Jensen, K. F.; Bawendi, M. G. *J. Phys. Chem. B* **1997**, *101*, 9463–9475. (b) Talapin, D. V.; Rogach, A. L.; Kornowski, A.; Haase, M.; Weller, H. *Nano Lett.* **2001**, *1*, 207–211. (c) Zhong, X.; Xie, R.; Zhang, Y.; Basche, T.; Knoll, W. *Chem. Mater.* **2005**, *17*, 4038–4042.
(3) (a) Pankhurst, Q. A.; Connolly, J.; Jones, S. K.; Dobson, J. *J. Appl. Phys. D: Appl. Phys.* **2003**, *36*, R167. (b) Tartaj, P.; Morales, M. P.; Veintemillas-Verdaguer, S.; Gonzales-Carreno, T.; Serna, C. J. *J. Appl. Phys. D: Appl. Phys.* **2003**, *36*, R182. (c) Berry, C. C.; Curtis, A. S. G. *J. Appl. Phys. D: Appl. Phys.* **2003**, *36*, R198.
(4) (a) Streffer, C.; Vaupel, P.; Hahn, G. M. *Biological Basis of Oncologic Thermo-therapy*; Springer: Berlin, 1990. (b) Jordan, A.; Scholz, R.; Wust, P.; Fähling, H.; Felix, R. *J. Magn. Magn. Mater.* **1999**, *201*, 413–419.
(5) (a) Langer, R. *Nature* **1998**, *392*, 5–10. (b) Duncan, R. *Nat. Rev. Drug Discov.* **2003**, *2*, 347–360.
(6) (a) Kang, H. W.; Josephson, L.; Petrovsky, A.; Weissleder, R.; Bogdanov, A., Jr. *Bioconjugate Chem.* **2002**, *13*, 122–127. (b) Schotter, J.; Kamp, P. B.; Becker, A.; Pühler, A.; Brinkmann, D.; Schepper, W.; Brückl, H.; Reiss, G. *IEEE Trans. Magn.* **2002**, *38*, 3365–3368. (c) Brzeska, M.; Panhorst, M.; Kamp, P. B.; Schotter, J.; Reiss, G.; Pühler, A.; Becker, A.; Brückl, H. *J. Biotechnol.* **2004**, *112*, 25–33.
(7) (a) Wang, L.; Luo, J.; Maye, M. M.; Fan, Q.; Rendeng, Q.; Engelhard, M. H.; Wang, C.; Lin, Y.; Zhong, C.-J. *J. Mater. Chem.* **2005**, *15*, 1821–1832. (b) Wang, L.; Luo, J.; Fan, Q.; Suzuki, M.; Suzuki, I. S.; Engelhard, M. H.; Lin, Y.; Kim, N.; Wang, J. Q.; Zhong, C.-J. *J. Phys. Chem. B* **2005**, *109*, 21593–21601.
(8) Philipse, A. P.; van Bruggen, M. P. B.; Pathmamanoharan, C. *Langmuir* **1994**, *10*, 92–99.

10.1021/cm7029954 CCC: $40.75
Published on Web 05/08/2008

The necessary surface modification of nanoparticles can be achieved by two methods: grafting of organic groups to the surface of nanomaterials after synthesis (postfunctionalization)[9] and in situ modification of nanomaterials by organic compounds (in situ functionalization).[10] In situ functionalization can be used, e.g., for Au nanoparticles which are synthesized typically in the presence of thiolate ligands.[11] Postfunctionalization is most particularly useful for particles prepared by high-temperature methods in hydrophobic solvents, including MFe_2O_4 (M = Co, Mn, Fe)[12] or CdSe,[13] thereby precluding incorporation of chemical functionality with organic ligands.[14]

Our approach presented in this contribution is to use a reactive polymeric ligand which is very versatile for postfunctionalization of surfaces. The modularity of the copolymer which is composed of several independent building blocks provides the basis of a comprehensive toolbox to tailor the surface functionality of metal, sulfide, or oxide nanoparticles in almost any desired manner for construction of supramolecular assemblies of organic−inorganic hybrid nanomaterials. After functionalization a pronounced chelate effect of the polymeric ligand imparts chemical stability, while solubility in various solvents can be obtained by an additional outer−polar or apolar−group. An important water-soluble ligand that has been used by us and others is poly(ethylene glycol),[15] whereas for apolar solvents simple alkyl groups are appropriate. If needed, optical detectability can be achieved by attaching a fluorescent ligand to the surface-bound polymer[16] or using a silica surface coating.[17] A novel aspect of this work is to utilize an immobilized active biocatalyst for fabrication of a protective silica coating around γ-Fe_2O_3 (maghemite) nanoparticles.

In nature, several classes of biosilicifying organisms process soluble silicon to generate hierarchically organized ornate biogenic silica structures under mild conditions of pH and temperature, and they exert precise control in shaping biosilica.[18] Recently we reported that silicatein, an enzyme involved in the biosilicification processes in these marine sponges, can be immobilized onto self-assembled monolayers, and we demonstrated the integrity and catalytic activity of surface-bound silicatein through formation of SiO_2 from tetraethoxysilane (TEOS)[19] and ZrO_2 from ZrF_6^{2-} as respective precursors.[20] Here we report a procedure for fabrication of a silica coating on γ-Fe_2O_3 nanoparticles by copolymerization of TEOS catalyzed by immobilized his-tagged recombinant silicatein.

Experimental Section

Materials. Tetraethoxysilane (TEOS) (>99.9%) was obtained from Sigma-Aldrich (Taufkirchen; Germany), N^{ϵ}-benzyloxycarbonyl L-lysine *tert*-butyl ester (#26239-55-4; 99%) was obtained from Acros (Geel; Belgium), dimethylformamide (DMF) was obtained from Riedel-de Haën (Seelze; Germany), Cy3-conjugated $F(ab')_2$ goat antirabbit IgG was obtained from Jackson ImmunoResearch (Cambridgshire CB7 5UE; U.K.), $Fe(CO)_5$ (99.50%), lauric acid (99.50%), 2,6-di-*tert*-butyl-4-methylphenol (99%), 2,6-lutidine (99%), AIBN (98%), 1,4-dioxane (99%), 3-hydroxytyramine hydrochloride (99%), triethylamine (99%), pentafluorophenol (99+%), $NiSO_4$ (99%), NaOH (97+%, pellets), NaCl (99+%), 3-(*N*-morpholino)propane sulfonic acid (MOPS), *n*-octane (99+%), toluene (99.5%), and dichloromethane (99.8%, water < 50 ppm, extra dry) were purchased from Acros, Germany. Dioctyl ether (99.5%), acryloyl chloride (98%), N_{α},N_{α}-bis(carboxymethyl)-L-lysine hydrate (>97.0%), and dehydrated trimethylamine *N*-oxide (98%) were obtained from Sigma-Aldrich, Germany.

Physical Characterization. *Mössbauer Spectroscopy.* Mössbauer measurements of γ-Fe_2O_3 powder samples were performed in transmission geometry using a constant-acceleration spectrometer and a helium bath cryostat. ^{57}Fe Mössbauer spectra were recorded between room temperature and 4.2 K using a 50 mCi source ^{57}Co(Rh). The Recoil 1.03 Mössbauer Analysis Software was used to fit the experimental spectra.[21] Isomer shift values are quoted relative to α-Fe at 293 K.

Magnetic Susceptibility Measurements. The magnetic susceptibilities of powder samples were measured with a SQUID magnetometer (Quantum Design).

Electron Microscopy. The products were characterized using transmission electron microscopy (TEM) using a Philips 420 instrument with an acceleration voltage of 120 kV or a Philips TECNAI F30 electron microscope (field-emission gun, 300 kV extraction voltage) as well as scanning electron microscopy (LEO 1530 Field emission SEM, 6 kV extraction voltage).

Infrared Spectroscopy. Infrared spectroscopy was performed using a Mattson Instruments 2030 Galaxy-FT-IR spectrometer.

(9) Kickelbick, G.; Schubert, U. In *Synthesis, Functionalization and Surface Treatment of Nanoparticles*; Baraton, M.-I., Ed.; American Scientific Publishers: Stevenson Ranch, CA, 2003.

(10) Sanchez, C.; Soler-Illia, G.; Ribot, F.; Lalot, T.; Mayer, C. R.; Cabuil, V. *Chem. Mater.* **2001**, *13*, 3061–3083. (b) Anderson, M.; Österlund, L.; Ljungström, S.; Palmqvist, A. *J. Phys. Chem. B* **2002**, *106*, 10674–10679. (c) Yin, S.; Aita, Y.; Komatsu, M.; Wang, J.; Tang, Q.; Sato, S. *J. Mater. Chem.* **2005**, *15*, 674–682.

(11) (a) Brust, M.; Walker, M.; Betell, D.; Schiffrin, J.; Whyman, R. *J. Chem. Soc., Chem. Commun.* **1994**, 801–802. (b) Bartz, M.; Weber, N.; Küther, J.; Seshadri, R.; Tremel, W. *J. Chem. Soc., Chem. Commun.* **1999**, 2085–2086. (c) Templeton, A. C.; Wuelfing, W. P.; Murray, R. R. *Acc. Chem. Res.* **2000**, *33*, 27–36.

(12) (a) Hyeon, T.; Lee, S. S.; Park, Y.; Chung, H. B. *J. Am. Chem. Soc.* **2001**, *123*, 12798–12801. (b) Park, J.; An, K.; Hwang, Y.; Park, J. G.; Noh, H. J.; Kim, J. Y.; Park, J. H.; Hwang, N. M.; Hyeon, T. *Nat. Mater.* **2004**, *3*, 891–895. (c) Sun, S.; Murray, C. B.; Weller, D.; Folks, L.; Moser, A. *Science* **2000**, *287*, 1989–1992.

(13) Gittins, D. I.; Caruso, F. *Angew. Chem., Int. Ed.* **2001**, *40*, 3001–3004.

(14) (a) Xu, C.; Xu, K.; Gu, H.; Zhong, X.; Guo, Z.; Xu, B. *J. Am. Chem. Soc.* **2004**, *126*, 3392–3393. (b) Xu, C.; Xu, K.; Gu, H.; Zheng, R.; Liu, H.; Zhang, X.; Guo, Z.; Xu, B. *J. Am. Chem. Soc.* **2004**, *126*, 3392–3393. (c) Hong, R.; Fischer, N. O.; Emrick, T.; Rotello, V. M. *Chem. Mater.* **2005**, *17*, 4617–4621.

(15) (a) Bartz, M.; Küther, J.; Nelles, G.; Weber, N.; Seshadri, R.; Tremel, W. *J. Mater. Chem.* **1999**, 1121–1125. (b) Foos, E. E.; Snow, A. W.; Twigg, M. E.; Ancona, M. G. *Chem. Mater.* **2002**, *14*, 2401–2408.

(16) Tahir, M. N.; Eberhardt, M.; Theato, P.; Faiβ, S.; Janshoff, A.; Gorelik, T.; Kolb, U.; Tremel, W. *Angew Chem., Int. Ed.* **2006**, *45*, 908–912.

(17) Medintz, I. L.; Uyeda, H. T.; Goldman, E. R.; Matoussi, H. *Nat. Mater.* **2005**, *4*, 435–436.

(18) (a) Shimizu, K.; Cha, J. N.; Stucky, G. D.; Morse, D. E. *Proc. Natl. Acad. Sci. U.S.A.* **1998**, *95*, 6234–6238. (b) Krasko, A.; Lorenz, B.; Batel, R.; Schröder, H. C.; Müller, I. M.; Müller, W. E. G. *Eur. J. Biochem.* **2000**, *267*, 4878–4887. (c) Müller, W. E. G.; Belikov, S. I.; Tremel, W.; Gamulin, V.; Perry, C. C.; Boreiko, A.; Schröder, H. C. *Micron* **2006**, *37*, 107–120.

(19) Tahir, M. N.; Théato, P.; Müller, W. E.G.; Schröder, H. C.; Janshoff, A.; Zhang, J.; Huth, J.; Tremel, W. *Chem. Commun.* **2004**, 2848–2849.

(20) Tahir, M. N.; Gorgeshvili, L.; Krasko, A.; Schröder, H. C.; Müller, W. E. G.; Tremel, W. *Chem. Commun.* **2005**, 5533–5535.

(21) Lagarec, K.; Rancourt, D. G. *Nucl. Instrum. Methods Phys. Res., Sect. B* **1997**, *129*, 266–270.

(22) (a) Eberhardt, M.; Mruk, R.; Zentel, R.; Theato, P. *Eur. Polym. J.* **2005**, *41*, 1569–1575. (b) Eberhardt, M.; Theato, P. *Macromol. Rapid Commun.* **2005**, *26*, 1488–1493.

Light Microscopy. Fluorescence analysis was performed with an Olympus AHBT3 light microscope together with an AH3-RFC reflected light fluorescence attachment at the emission wavelength of 546 nm (filter G).

Iron Oxide Nanoparticles and Functionalization. Nanocrystallites of iron oxide were synthesized as reported in the literature.[12] In short, iron pentacarbonyl, $Fe(CO)_5$ (0.2 mL, 1.52 mmol), was injected into a solution containing 0.91 g of lauric acid (4.56 mmol), 7 mL of octyl ether, and 0.57 g of dehydrated trimethylamine *N*-oxide $(CH_3)_3NO$ (7.60 mmol) at 100 °C in an argon atmosphere with vigorous stirring. As soon as $Fe(CO)_5$ was injected into the mixture, the temperature rose to 120 °C and the solution became dark red, which indicated successful oxidation of $Fe(CO)_5$. The reaction mixture was then stirred for 1 h at 120 °C, and the solution was slowly heated to reflux. The solution color gradually became black, indicating that nanoparticles were being formed. After refluxing for 1 h, the solution was cooled to room temperature, and a black precipitate was obtained upon adding excess ethanol and centrifuging. The precipitate can be easily redispersed in octane or toluene. Phase identification of the naked iron oxide nanoparticles was carried out using transmission electron microscopy (TEM), magnetic susceptibility (SQUID) measurements, and Mössbauer spectroscopy.

Synthesis of the Reactive Polymer. The polymer poly(pentafluorophenyl acrylate) was synthesized by RAFT polymerization of pentafluorophenyl methacrylate as stated in ref 22. GPC analysis of the obtained polymer (THF, light scattering detection) gave the following values: M_n = 29.7 kg/mol; M_w = 58.5 kg/mol, where the number of repeating units (236) is based on the M_w value. The polymer contains 20% dopamine (47 units) and 80% NTA (189 units per molecule of polymer).

(a) Synthesis of Monomer Pentafluorophenyl Acrylate. A 5.4 g (29.3 mmol) amount of pentafluorophenol and a few percent of 2,6-di-*tert*-butyl-4-methyl phenol were dissolved in 60 mL of dry dichloromethane. To the cold mixture 3.5 mL of 2,6-lutidine and 2.9 mL (31.9 mmol) of acryloyl chloride were added dropwise. The solution was stirred for 3 h at 0 °C and then kept at room temperature for 8 h. After evaporating the solvent under reduced pressure the salt was filtered off and product distilled under reduced pressure yielding pure pentafluorophenyl acrylate (0.05 mbar, bp 27 °C). ^{1}H NMR: δ[ppm] = 6.70, 6.36, 6.16. ^{19}F NMR: δ[ppm] = −162.77, −158.39, −153.02.

(b) Polymerization. The monomer and 0.01 mol % of AIBN were dissolved in dry dioxane, degassed, and stirred for 24 h at 80 °C. The resulting homopolymer was precipitated in cold diethyl ether, yielding a polymer with molecular weight M_n = 24.0 kg/mol and M_w = 37.1 kg/mol (PDI = 15). ^{1}H NMR: δ[ppm] = 3.07, 2.09. ^{19}F NMR: δ[ppm] = −162.59, −157.15, −153.56.

(c) NTA−Dopamine Polymer. For the synthesis of the NTA−dopamine polymer, PFA (110 mg, 0.46 mmol repeating units) was dissolved in dry DMF (3 mL). A solution of 3-hydroxytyramine hydrochloride (dopamine) (10.5 mg, 0.055 mmol) in DMF (1.5 mL) and triethylamine (0.1 mL) was added, and the clear mixture stirred for 1 h at 50 °C. A solution of amino-functionalized NTA (120 mg, 0.46 mmol) in MilliQ water (0.9 mL) and triethylamine (2.1 mL) was then added, and the resulting mixture was kept at 50 °C for 6 h. The slight excess of NTA was used to ensure complete conversion of the remaining active ester groups. After removal of the DMF, the solution was adjusted to pH 3 and the crude viscous product cleaned by dialysis in MilliQ water, isolated, and finally dried in a vacuum oven at 40 °C for 1 h to give 64 mg of a white polymeric powder. Total repeat units = 236, dopamine composition = 20% (47 units per molecule of polymer), NTA composition = 80% (189 units per molecule of polymer). ^{1}H NMR: δ[ppm] = 8.17, 7.17, 6.87, 3.42, 3.29, 3.06, 2.87, 2.72, 2.49, 1.57, 1.36, 1.16 (the corresponding ^{1}H NMR spectrum is given as Figure S1, Supporting Information).

NTA−Dopamine Polymer Functionalization. A 15 mg amount of the above synthesized γ-Fe_2O_3 nanocrystallites were treated with 50 mg of the reactive polymer dissolved in *N*,*N*-dimethylformamide (DMF). The reaction was carried under an inert atmosphere and vigorous mechanical stirring at 50 °C for 12 h followed by cooling the reaction system to room temperature. To remove unbound polymer the coated magnetic particles in the solution were extracted by a magnetic particle concentrator (Dynal MPC1-50, Dynal Biotech, France) at room temperature. The isolated magnetic nanoparticles were washed with DMF, ensuring removal of unreacted polymer. The samples were analyzed by transmission electron microscopy (TEM) and high-resolution transmission electron microscope (HRTEM).

Recombinant Silicatein and Preparation of Antibodies. Recombinant silicatein was prepared in *Escherichia coli* and purified as described. The recombinant protein contained a His-tag as described elsewhere.[18b] Polyclonal antibodies (PoAb-aSILIC) were raised against purified, recombinant silicatein in female rabbits (White New Zealand). The titer of the PoAb-aSILIC antibodies were >1:3000.[23]

Silicatein Immobilization onto Ni−NTA Polymer-Functionalized γ-Fe_2O_3. To immobilize silicatein, the functionalized γ-Fe_2O_3 nanocrystals were treated with 1 mmol of an aqueous solution of NaOH for 30−45 min under continuous stirring. The mixture was centrifuged and washed with deionized MilliQ water (18.2Ω), and the functionalized nanocrystals were rotated in a solution of $NiSO_4$ (40 mmol) for 1 h. The iron oxide nanocrystals containing complexed Ni^{2+} ions were then removed, washed with a solution of NaCl (150 mmol) and deionized water, and dried in a stream of N_2. A solution of silicatein (30 nmol) in 3-(*N*-morpholino)propane sulfonic acid (MOPS) buffer was then added to the Ni^{2+}-bound γ-Fe_2O_3 nanocrystals, and the mixture was shaken gently for 1 h. The silicatein-immobilized γ-Fe_2O_3 nanocrystals were washed with MOPS buffer and deionized water to remove unbound protein.

Immunostaining of the Silicatein-Functionalized γ-Fe_2O_3 Nanoparticles. The silicatein immobilization onto the above functionalized iron oxide nanocrystals was monitored by incubating the primary antisilicatein polyclonal antibody PoAb-aSILIC (1:1000 dilution) in a 2.5% blocking solution (PBS/BSA) for 1 h at room temperature. The sample was washed several times using TBS-T ([Tris-buffered saline], pH 7.5 + 0.05% Tween-20) for 5 min followed by secondary antibody, Cy-3 conjugated goat antirabbit IgG (1:2000 dilution) incubation in 2.5% blocking solution for 1 h at ambient temperature, followed by washing with PBS (phosphate-buffered saline). Controls were performed using polymer-derivatized nanoparticles either with immobilized recombinant silicatein and preimmune serum prepared in a solution (1:1000 dilution) of BSA/PBS (2.5%) or in the absence of silicatein. The fluorescence analysis was performed with an Olympus AHBT3 light microscope together with an AH3-RFC reflected light fluorescence attachment at the emission wavelength of 546 nm (filter G).

Silica Coating onto Silicatein-Immobilized γ-Fe_2O_3. Nanocrystallites with immobilized silicatein were treated with a solution of TEOS (60 μM, MOPS buffer 20 mM, pH 7.0) at room temperature for 3 h to obtain a fine coating of silica.[24] Excess TEOS was washed away with ethanol followed by MOPS buffer and

(23) Müller, W. E.G.; Rothenberger, M.; Boreiko, A.; Tremel, W.; Reiber, A.; Schröder, H. C. *Cell. Tiss. Res.* **2005**, *321*, 285.
(24) Tahir, M. N.; Théato, P.; Müller, W. E. G.; Schröder, H. C.; Boreiko, A.; Faiss, S.; Janshoff, A.; Huth, J.; Tremel, W. *Chem. Commun.* **2005**, 5533–5535.

Scheme 1. General Scheme of Functionalization of Maghemite (γ-Fe_2O_3) Nanoparticles Followed by Immobilization of Recombinant Slicatein and Formation of Silica Coating

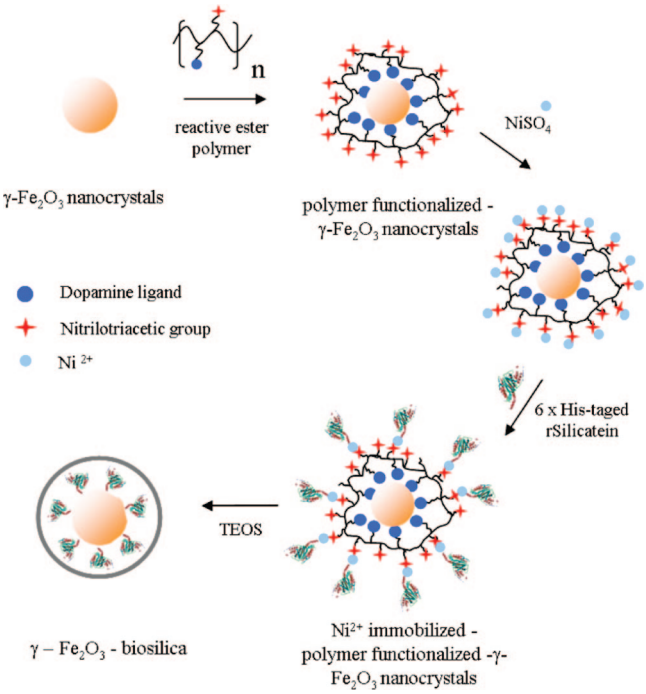

deionized water making use ofthe magnetic properties of the particles. The γ-Fe_2O_3@silica particles were characterized by TEM and scanning transmission electron microscopy (STEM) coupled to an electron-dispersive X-rays spectroscopy (EDX) for elemental analysis.

Results and Discussion

To demonstrate the easy and general utility of the fabrication procedure, we first describe the synthesis of the γ-Fe_2O_3 nanoparticles and the polymeric surface ligand, show the surface functionalization using a linker group, polymer, and protein, and finally demonstrate the assembly of a fine coating of magnetic particles by silicatein-mediated polymerization of TEOS. The individual steps are illustrated in Scheme 1.

Nanocrystallites of iron oxide were synthesized by thermal decomposition of iron pentacarbonyl as reported in the literature.[12] Phase identification of the naked iron oxide nanoparticles was carried out using transmission electron microscopy (TEM), magnetic susceptibility (SQUID) measurements, and Mössbauer spectroscopy. The TEM image of naked γ-Fe_2O_3 nanoparticles in Figure 1a reveals well-separated, spherical, and relatively uniform sized nanocrystals with diameters ranging from 5 to 10 nm. Figure 1b shows a high-resolution TEM (HRTEM) image of a single nanocrystal with an interlayer *d* spacing of 0.25 nm which can be attributed to the (311) plane of maghemite.

Maghemite (γ-Fe_2O_3) and magnetite (Fe_3O_4) cannot be easily distinguished by Mössbauer spectroscopy as both of them adopt an inverse spinel structure. The Mössbauer spectrum of the unfunctionalized nanoparticles at room temperature is shown in Figure 2a. As maghemite is superparamagnetic for particles sizes <10 nm the Mössbauer spectrum contains only a single doublet. Whereas the isomer shift IS = 0.37(3) mm s^{-1}corresponds to that of bulk maghemite, the quadrupole splitting QS = 0.70(1) mms^{-1} is quite large and deviates from the literature value[25] due to large number of surface atoms. The hysteresis loop for the γ-Fe_2O_3 nanocrystallites in Figure 2 b indicates superparamagnetic behavior without any hysteresis at room temperature. The magnetization data indicate a magnetization of 65 emu/g for the γ-Fe_2O_3nanoparticles at 40 kOe. For these small particle sizes Mössbauer spectra consisting of only one doublet have been reported.[26]

Subsequently, the γ-Fe_2O_3 nanoparticles were functionalized using a multidentate functional copolymer[27] (Scheme 2) carrying catecholate groups as surface binding ligands for iron oxide nanoparticles and nitrilotriacetic (NTA) groups for the attachment of his-tagged proteins (Scheme 1). The average crystallite size of particles with functional polymer coating was estimated using TEM. Figure 1c shows that the functionalized nanocrystals do not form aggregates and that the size did not change upon ligand exchange within the limits of TEM accuracy. The presence of charge at the polymer end confers water solubility of the nanoparticles through interparticle repulsion.[28]

Figure 3 shows Fourier transform infrared (FTIR) spectra of naked γ-Fe_2O_3 nanoparticles, polymeric ligand, and polymer-functionalized γ-Fe_2O_3 nanoparticles. The presence of three strong absorption bands at 2959, 2920, and 2850 cm^{-1} in naked iron oxide nanoparticles correspond to the CH_3 asymmetric as well as symmetric stretching frequencies due to the surfactant used in synthesis. The respective absorption bands (arrows indicated in the figure) at 1738 and 1653 cm^{-1} in the spectra of polymer-functionalized nanocrystals correspond to the carboxylic (C═O) NTA groups and C═O of amide groups confirming the polymer binding. The absorption bands due to the C═C−H stretching frequency of the catecholate moiety overlaps with a broad absorption, centered at 3444 cm^{-1} due to the COOH functionality of the NTA groups in functionalized nanoparticles.

After binding of the polymer, Ni(II) complexation and subsequent immobilization of recombinant−silicatein onto the polymer-functionalized nanoparticles surface was carried out and monitored by immunostaining. Polyclonal antibodies (PoAb-aSilic) raised against silicatein were used for detection of the immobilized protein.[23,29] The particles with immobilized silicatein were reacted with a solution containing PoAb-aSilic and secondary goat antirabbit antibodies fluorophore-labeled (Cy3-label) (Figure 4b). The immunocomplexes were analyzed under an epiflourescent microscope with an emission wavelength of 546 nm. The surface-bound silicatein was detected with the help of primary antibodies which upon detection by Cy3-conjugated secondary anti-

(25) Haneda, K.; Morrish, A. H. *Phys. Lett.* **1977**, *64A*, 779–782.
(26) Taylor, R. M.; Schwertmann, U. *Clay Miner.* **1974**, *10*, 299–310.
(27) Shukoor, M. I.; Natalio, F.; Ksenofontov, V.; Tahir, M. N.; Eberhardt, M.; Theato, P.; Schröder, H. C.; Müller, W. E. G.; Tremel, W. *Small* **2007**, *3*, 1374–1377.
(28) Pellegrino, T.; Kudera, S.; Liedl, T.; Javier, A. M.; Manna, L.; Parak, W. J. *Small* **2005**, *1*, 48–63.
(29) Tahir, M. N.; GorelikAngew, T.; Kolb, U.; Schröder, H.-C.; Müller, W. E. G.; Tremel, W. *Angew. Chem., Int. Ed.* **2006**, *45*, 4803–4809.

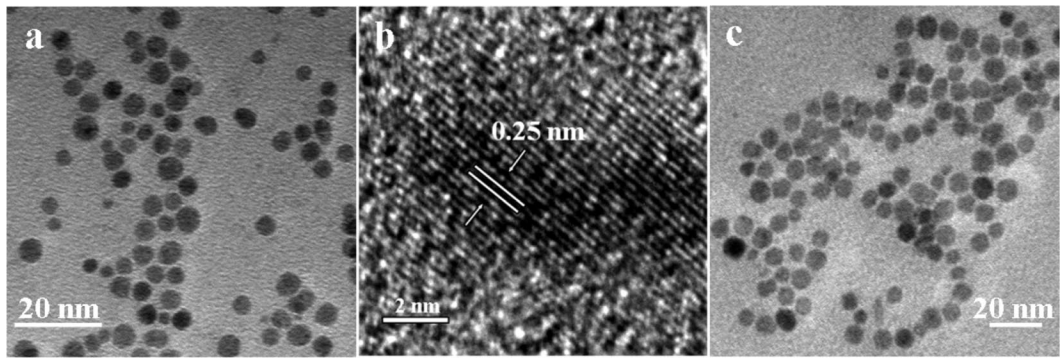

Figure 1. (a) Transmission electron microscope (TEM) and (b) high-resolution transmission electron microscope (HRTEM) image of a naked γ-Fe_2O_3 nanoparticle. (c) TEM image of polymer-functionalized nanoparticles.

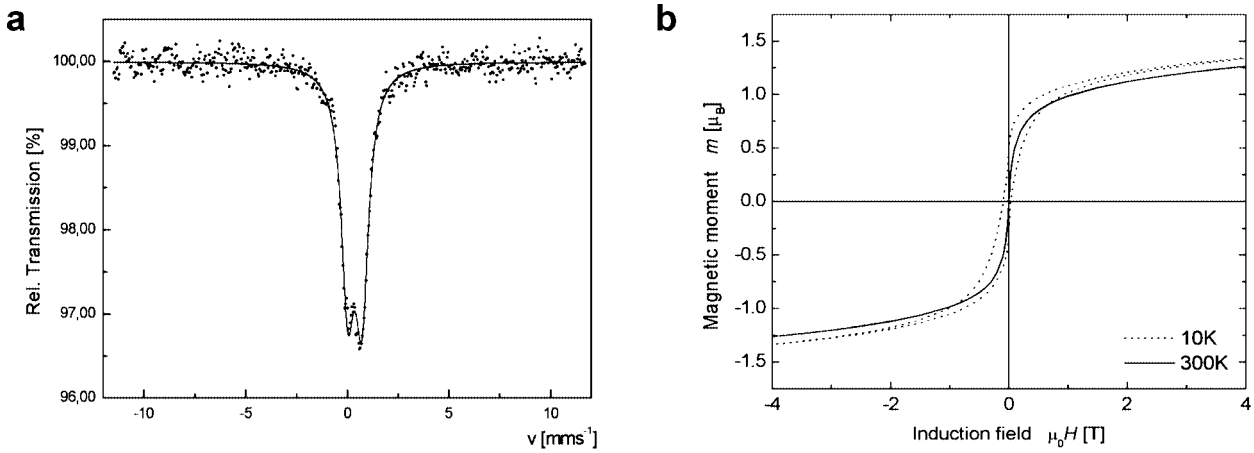

Figure 2. (a) Mössbauer spectrum of γ-Fe_2O_3 nanoparticles at room temperature. (b) Magnetization curve of γ-Fe_2O_3 nanoparticles at 300 and 10 K.

Scheme 2. Structure of the Polymer-Containing Catecholate and NTA Groups

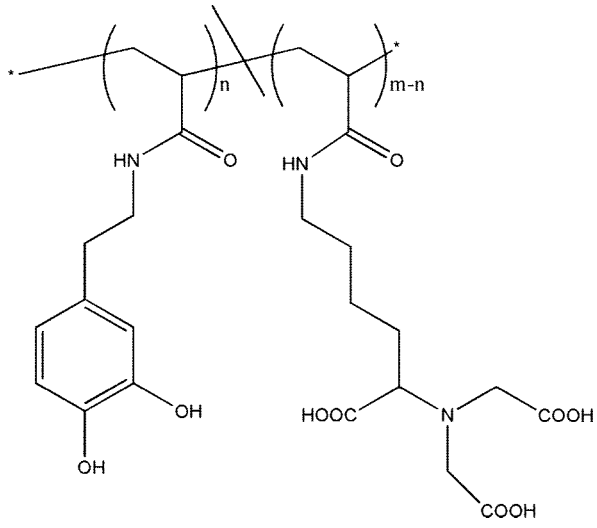

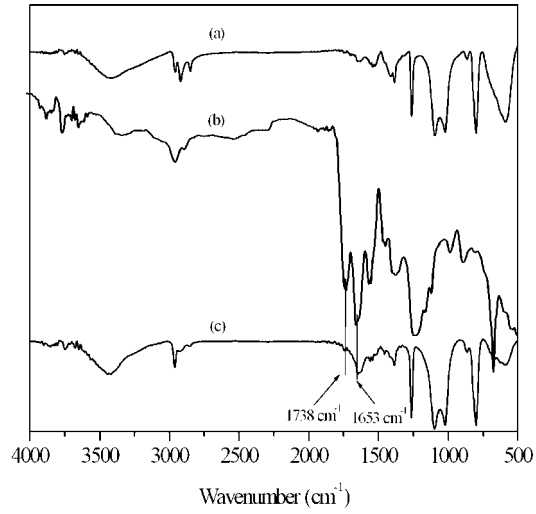

Figure 3. FT-IR spectrum of (a) naked γ-Fe_2O_3 nanoparticles, (b) pure polymeric ligand, and (c) polymer-functionalized γ-Fe_2O_3 nanoparticles.

bodies result in a red fluorescent signal (Figure 4b). Naked γ-Fe_2O_3 nanoparticles observed under the optical microscope show no fluorescence (not shown). As a control, silicatein-immobilized nanoparticles incubated with a solution prepared with preimmune serum show no fluorescence. (Figure 4a).[23] On the other hand, a second control set was performed where NTA−polymer-functionalized iron oxide nanoparticles with complexed Ni(II) were incubated with PoAb-aSilic in the absence of recombinant silicatein. Here no fluorescence signal was detected (not shown).

After silicatein immobilization, the nanoparticles were incubated with the alkoxide precursor (TEOS) to induce formation of a biocatalytically templated silica shell. Shell formation was analyzed by transmission electron microscopy (TEM) and scanning transmission electron microscopy (STEM), and the silica content was determined by elemental analysis using EDX. Figure 5a shows an overview image of the sample. Figure 5b and 5c shows the HRTEM and STEM images of silica-coated polymer-functionalized iron oxide nanoparticles. The brightness in the image reflects the

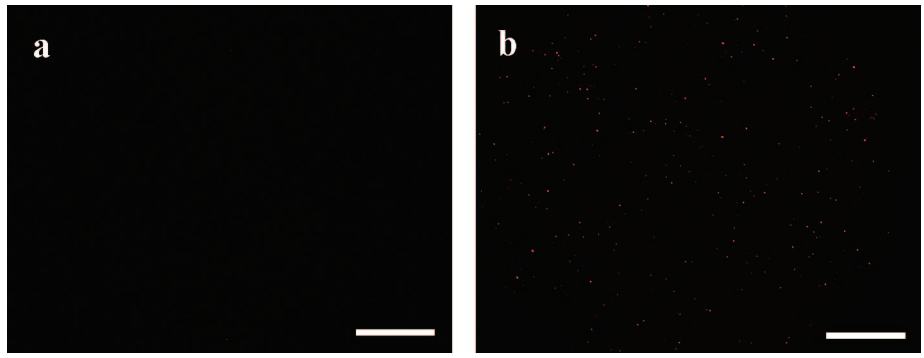

Figure 4. Fluorescence microscope images of silicatein immobilized onto polymer-functionalized γ-Fe_2O_3nanoparticles (a) incubated with preimmune serum and (b) polyclonal antibodies PoAb-aSilic (scale bars: 20 μm).

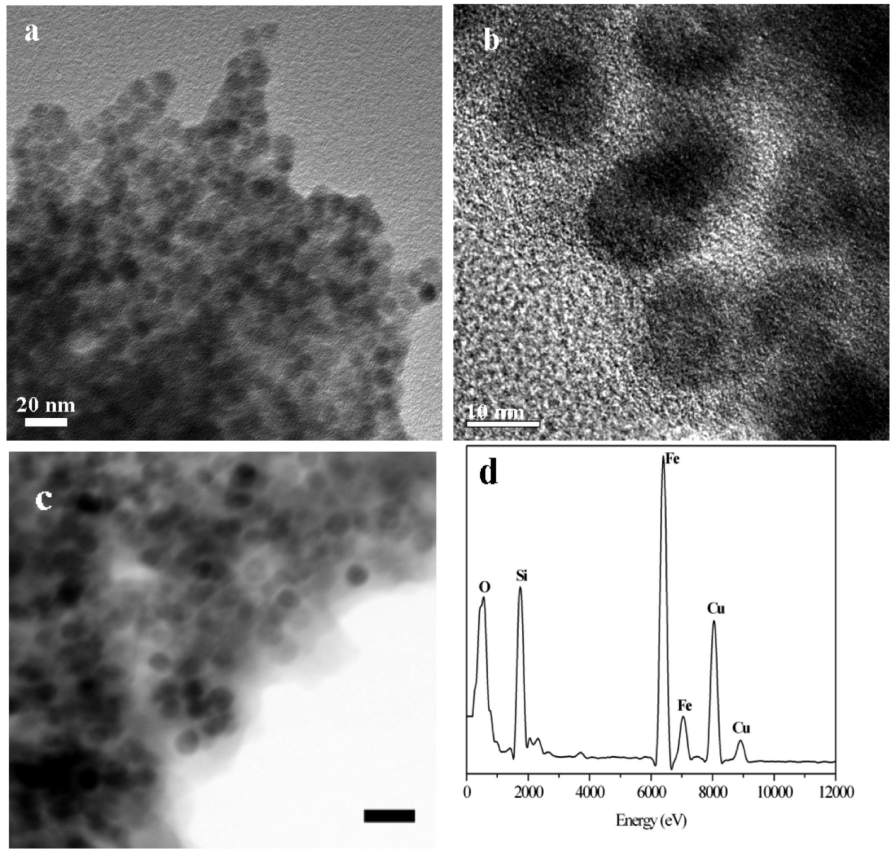

Figure 5. Silica-coated polymer-functionalized γ-Fe_2O_3 nanocrystallites: (a, b) TEM and HRTEM images, (c) scanning transmission electron microscope (STEM) image (scale bar: 20 nm), and (d) corresponding EDX spectrum.

intensity of scattered electrons from different areas of the substance, and it is proportional to the atomic number (Z).[30] In the corresponding bright-mode image (Figure 5c) the γ-Fe_2O_3 nanoparticles appear darker. In order to prove the presence of the silica, an elemental analysis of the sample was performed using electron-dispersive X-rays spectroscopy (EDX). The EDX spectrum in Figure 5d proves the presence of iron, silicon, and oxygen. The final product displays a hierarchical γ-Fe_2O_3@polymer@silicatein@SiO_2 core−shell-type structure.

The enzymatic activity of free silicatein has been demonstrated earlier.[31] In order to confirm the catalytic activity of the surface-bound silicatein for deposition of silica two comparative sets of experiments were performed as controls. Ni(II)-complexed NTA-polymer functionalized γ-Fe_2O_3 nanoparticles were incubated with the alkoxide precursor (TEOS) for 4 h, at room temperature, where no silica shell formation was observed but particles were agglomerated. However, under similar conditions, when TEOS incubation was performed for a longer period (24 h) a clear unstructured and bulky deposition of silica at the surfaces of the γ-Fe_2O_3 nanoparticles could be observed (Figure S2, Supporting Information). Formation of the silica mantle after immobilization of silicatein onto the surface through the

(30) Nellist, D.; Pennycook, S. J. *Ultramicroscopy* **1999**, *78*, 111–124.

(31) (a) Zhou, Y.; Shimizu, K.; Cha, J. N.; Stucky, G. D.; Morse, D. E. *Angew. Chem., Int. Ed.* **1999**, *38*, 779–782. (b) Müller, W. E. G.; Schlossmacher, U.; Wang, X.; Boreiko, A.; Brandt, D.; Wolf, S. E.; Tremel, W.; Schröder, H. C. *FEBS J.* **2008**, *275*, 362–370.

Ni−NTA polymer binding indicates that the surface-bound protein is as a catalyst indeed responsible for faster formation of the outer silica layer through its polycondensating and enzymatic activity.

Conclusion and Outlook

We presented a novel bioinspired assembly of magnetic silica-coated γ-Fe_2O_3@SiO_2 nanoparticles. Polymer-functionalized γ-Fe_2O_3 surfaces can immobilize histidine-tagged silicatein using the efficient chelating properties with Ni^{2+}. The results presented here demonstrate that surface-bound silicatein, previously shown to be active for catalyzing and structurally directing the polycondensation of silicon alkoxides in solution as well as on surfaces, can catalyze deposition of a protective silica shell around magnetic oxide nanoparticles. Maghemite can therefore not be regarded as a template in a classical sense.[32] With respect to biomineralization, the results presented here indicate that surface binding of crystallization promotors such as silicatein may have an important impact on the morphology of the resulting products, e.g., through formation of hierachical assemblies such as layer by layer structures.

Acknowledgment. We acknowledge partial support from the Deutsche Forschungsgemeinschaft (DFG).

Supporting Information Available: NMR spectrum of the polymer (Figure S1) and TEM images of control experiments where silica deposition was attempted with polymer-coated γ-Fe_2O_3 nanocrystallites but without tagged silicatein (after 4 and 24 h) (PDF). This material is available free of charge via the Internet at http://pubs.acs.org.

CM7029954

(32) Many templates have been used for silica: (i) molecular templates for microporous silica, (ii) supramolecular templates for mesoporous silica, and (iii) polymers, peptides, or supramolecular aggregates. Pertinent references can be found in the following. (a) *Handbook of Porous Solids*; Schüth, F., Sing, K. S. W., Weitkamp, J., Eds.; Wiley-VCH: New York, 2002; Vol. 1, (5). (b) *Handbook of Biomineralization*; Baeuerlein, E., Ed.; Wiley-VCH: New York, 2007; Vol. *1*, (3).